Particle Size Distribution Characteristics within Different Regions of Mature Squall-line Based on the Analysis of Global Precipitation Measurement Dual-frequency Precipitation Radar Retrieval

Ziwei Zhu, Youcun Qi, Qing Cao, Donghuan Li, Zhe Zhang, Jie Cao, and Ming Xue

***Abstract*—Particle size distribution (PSD) characteristics of mature squall lines are investigated through global precipitation measurement (GPM) dual-frequency precipitation radar (DPR) measurements. These squall lines consist of a leading convective line (LC), a weak-echo transition (WT) region and a trailing stratiform (TS) region. Their PSD characteristics are quite different from the existing conceptual models of mature squall line, given that many small raindrops/ice particles are found in the WT region while in the TS region raindrops/ice particles are sparse. Analysis shows that it is likely due to the short distance from LC to WT, where more particles may be dispersed from LC region and fall into WT region but barely have time to grow in size. In the TS region further behind LC, the particles have more time to get larger. Analysis also reveals that the mesoscale updraft generally occurs at mid-to-high levels in the TS region so that aggregations and collisions-coalescences could be promoted to increase the particle size but decrease the particle number. Through the GPM PSD data analysis, a refined conceptual model of MCS with squall line is presented in this study.**

***Index Terms*—squall line, particle size distribution, dual-frequency precipitation radar, global precipitation measurement mission**

I. Introduction

A mesoscale convective system (MCS) is formed by a complex of deep convective cells, which produce widely spread precipitation on the order of 100 km or more. MCS's usually cause hazardous weather, such as high winds, hail, and even tornadoes accompanied with heavy rainfall. Flash floods are normally triggered, especially for long lived, slowly moving MCS's [1-4]. Studies on MCS's started with cloud photography in the 19th century, and its internal structures were revealed gradually as the advancement of observation instruments, especially since the emergence of radar meteorology in 1950s [5].

MCS prediction is still not accurate with current operational numerical prediction models [6]. Precise measurements of particle size distribution (PSD) are essential to improve the microphysical schemes for severe MCS forecasting. Disdrometer observations can provide the most reliable PSD information, and some results have been published [7-9]. However, disdrometers provide the PSD just near the ground surface, and one disdrometer could only measures one grid point. Considering the broad structure and spatial variation of MCS, it is very difficult to obtain spatially continuous PSD observation through disdrometers only. Wind profilers extend the PSD measurements in vertical direction relative to disdrometers, but are still not enough. For example, Cifelli et al (2000) [10] reported the results of PSD retrievals of eight MCS's in Darwin, Australia using dual-frequency wind profilers with a height range from 1.6 to 3.7 km (about 1 km below the 0 °C isotherm as noted in [10]), which could not detect the variation of hydrometeors from the storm top to the ground surface. Moreover, ground-based instruments have a large limitation making measurements in storms over ocean. It is still not very clear whether the mechanisms of MCS's in the ocean are different from those occurring over the land. Satellite could provide a better data source since it breaks the space and geographical restrictions. The Global Precipitation Measurement (GPM) Core Observatory—launched on 14 February 2014—carries the first dual-frequency space-borne precipitation radar (DPR). By radar retrieval with dual frequencies, namely Ku band (13.8 GHz) and Ka band (35.5 GHz), the DPR provides comprehensive three-dimensional storm structure [11]. It provides a new perspective to better understand the inner microphysics of the MCS.

As a typical type of MCS's, the squall line (hereafter squall-line MCS) has been of high interest because it is highly organized and easier for analysis and modeling [5]. Several conceptual models illustrating the kinematic, microphysical, and radar echo structure of squall-line MCS have been presented in the 1990s [12-14]. Furthermore, through a composite analysis conducted by combining 26 high-frequency rawinsondes, 2 wind profilers, 70 surface meso-network stations, 4 Doppler radars and 3 National Weather Service surveillance radars into a coordinate system, Biggerstaff and Houze (1991, hereafter BH91) [12] speculated that the hydrometeors could be advected from the convective line to the trailing stratiform region, and estimated that the PSDs near the surface of this area could be affected by the squall-line MCS. The current study tries to investigate the PSDs of squall-line

Ziwei Zhu, Youcun Qi, Donghuan Li and Zhe Zhang are with Key Laboratory of Water Cycle and Related Land Surface Processes, Institute of Geographic Sciences and Natural Resources Research, Chinese Academy of Sciences, Beijing, China. Ziwei Zhu is also with University of Chinese Academy of Sciences, Beijing, China. Qing Cao is with Enterprise Electronics Corporation, Enterprise, AL, USA.

Jie Cao is with Key Laboratory of Cloud-Precipitation Physics and Severe Storms (LACS), Institute of Atmospheric Physics, Chinese Academy of Sciences, Beijing, China

Ming Xue is with Center for analysis and prediction of storms and School of Meteorology, University of Oklahoma, Norman, OK 73072, USA

MCS based on GPM DPR observations, and makes a deep understanding of the PSDs in a squall-line MCS. The next section describes the data and methodology. Section III presents the new understanding of the PSDs in squall-line MCS. The last section summarizes the findings and makes an outlook for future works.

II. Data And Method

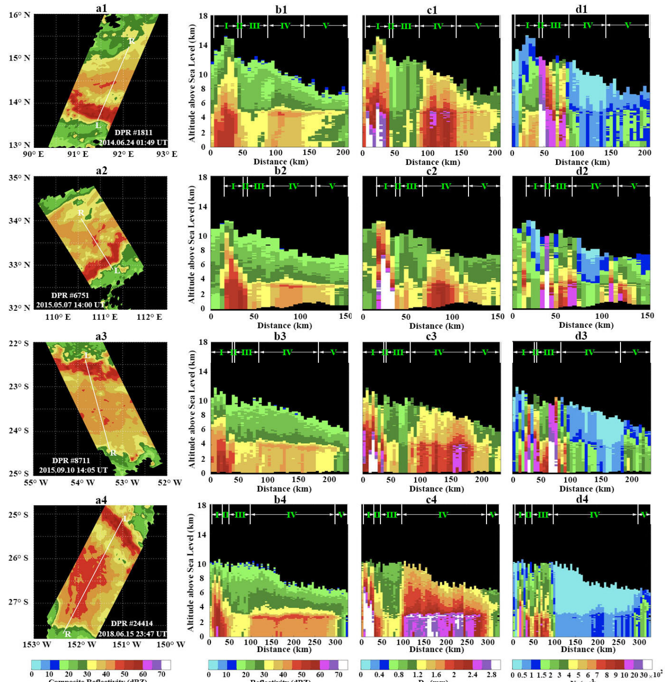

Figure 1. Four typical squall-line MCS events that occurred at land and ocean, northern and southern hemispheres and were observed by MS DPR. Column a: the composite reflectivity (Ku; corrected); columns b, c and d are the vertical cross sections of reflectivity (Ku; corrected), mass-weighted mean diameter (D_m) and number of precipitating particles along the white lines in column a. The letters "L" and "R" indicates the left and right ends of the vertical cross sections. Five different regions of the squall lines are marked in columns b, c and d. I: mature cells; II: old cells; III: transition zone; IV: heavy stratiform; V: stratiform tail.

The version 6 Matched Scan (MS) DPR PSD data were used to investigate the three-dimensional PSD characteristics of the squall-line MCS. GPM DPR operates at Ku and Ka band. The swath of Ku band is 245 km including 49 footprints, while only the central 125 km (25 footprints) is completely matched with Ka band measurements, i.e., MS. GPM DPR provides three-dimensional precipitation structure between 65°N and 65°S with the horizontal resolution of 5 km and

vertical resolution of 125 m, from altitude 22 km to the surface. Given this coverage, GPM DPR can potentially observe the evolution of a squall-line MCS and offer a high resolution three-dimensional retrieval of PSD information.

The DPR retrieval can be well done with a two-dimensional PSD model based on the raindrop scattering difference between two different frequencies [15]. It is assumed that the PSD can be characterized by two parameters, i.e., the normalized intercept parameter (N_w) and the mass-weighted mean diameter (D_m). First, the attenuation correction of the measured reflectivity factors is a necessary step to obtain the effective

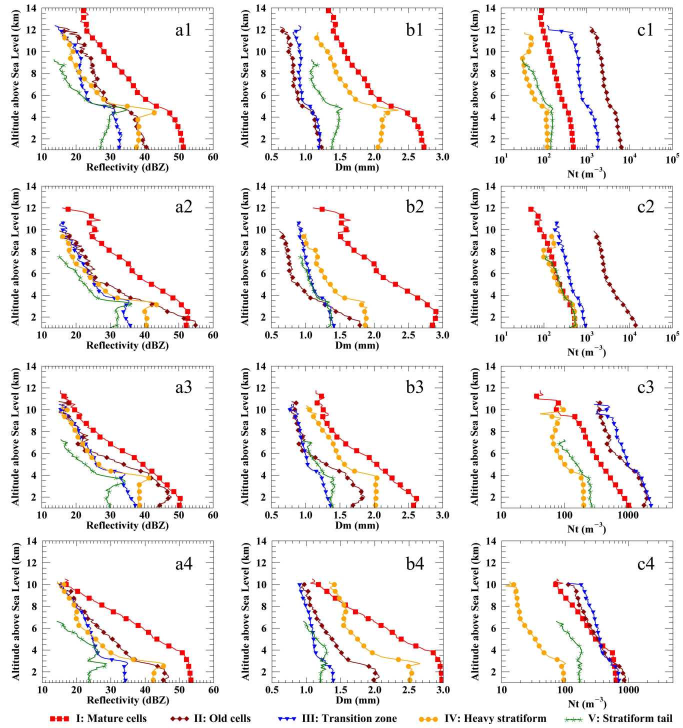

Figure 2. Mean vertical profiles of the Ku-band reflectivity (column a), D_m (column b) and N_t (column c) for the five different regions of squall lines divided in Figure 1. Each row represents the same squall line event as shown in Figure 1.

radar reflectivity factors (Z_e) at the dual frequencies. Then, the D_m can be uniquely determined by the dual frequency ratio (DFR) given:

$$Z_e = N_w F(D_m) \tag{1}$$

$$DFR = Z_e^{Ka}/Z_e^{Ku} = F^{Ka}(D_m)/F^{Ku}(D_m) \tag{2}$$

Where F is a function of D_m *[mm]* that expresses the scattering characteristics of precipitation particles at the given wavelength and the superscript Ka/Ku denotes the value for Ka/Ku band. Once the D_m is derived, the N_w $[m^{-3} \cdot mm^{-1}]$ can be solved by Eq. (1).The performance of PSD retrieval from the MS DPR observations has been validated in the previous studies [16-19]. It is confirmed that the DPR PSD parameters are reliable and have a high quality, and perform best among all GPM-based PSD products.

The scattering properties also depends the phase of particles, which are determined by identification of bright band in GPM DPR algorithm. The details will not be covered here but can be found in [15]. For liquid precipitation, PSD can be robustly expressed by a three-parameter gamma distribution function as:

$$N(D) = N_w f(\mu)\left(\frac{D}{D_m}\right)^{\mu} exp\left[-\frac{(4+\mu)D}{D_m}\right] \tag{3}$$

$$f(\mu)= \frac{6}{4^4}\frac{(\mu + 4)^{\mu+4}}{\Gamma(\mu + 4)} \tag{4}$$

where, the particle diameter and the corresponding number concentration are designated as D *[mm]* and $N(D)$ $[m^{-3} \cdot mm^{-1}]$, respectively. Γ denotes the gamma function. μ is the shape factor and is fixed at 3 in the DPR algorithm [21].

For precipitation particles in mixed or solid phase, the GPM DPR group assumes the PSD obey Eq. (3) when all the particles are melted to liquid drops [15], and D_m is defined for the equivalent particle diameter when melted. So, we have a more general relationship as:

$$N(D_{melt}) = N_w f(\mu)\left(\frac{D_{melt}}{D_m}\right)^{\mu} exp\left[-\frac{(4+\mu)D_{melt}}{D_m}\right] \quad (5)$$

Given the D_{melt} ranging from 0.1 to 8.0 mm, the distribution of the total number concentration (N_t) can be computed by integrating Eq. (3) as:

$$N_t = \int_{0.1}^{8} N(D_{melt}) d\,D_{melt} \quad (6)$$

Although the reliability of N_w has been demonstrated in many GPM validation efforts, the fact that N_w has larger uncertainties than Dm has also been reported [19, 20]. Therefore, on the PSD characteristics of squall line, the current analysis mainly focus on the relative differences among different regions, rather than give a quantitative conclusion. And, to better interpret the particle number difference in different MCS regions, the N_t, instead of N_w, is analyzed in the current study.

III. Results

The squall line structure is clearly visible from radar composite reflectivity (e.g., Figure 1a1-a4). Through looking over 26417 global scans of GPM DPR one by one, we have identified 1226 squall line events between 8 March 2014 and 31 October 2018. The 1226 events only include those that have complete squall line structure, i.e., both the quasi-linear convective cells and the trailing stratiform region are presented in MS DPR scans. After checking the 1226 squall lines, we have found that the PSD from the convective cells to the stratiform tail have very similar distribution to their counterparts in different events. The particles in the core convective region tend to have a large size while many particles with modest size are concentrated at the rear edge of convective region. For the trailing stratiform, the particles in the transition zone are small and dense while those in the heavy stratiform region are relatively larger and sparse. In order to illustrate the detailed PSD structure of the squall-line MCS and to show its PSD characteristics where it occurs, we picked up four well developed squall-line MCS's (Figure 1) occurring on land and sea from the southern and northern hemispheres, respectively. Noting that the analysis of the four events is consistent with all the 1226 events. The four squall-line MCS's occurring in the Bay of Bengal (row 1), China (row 2), Brazil (row 3) and the South Pacific (row 4) are chronologically shown in Figure 1. The Ku-band composite reflectivity (i.e., the maximum reflectivity among the vertical volume at each grid point) and the vertical section of reflectivity shown in column a and b has been corrected for the attenuation with the DPR algorithm. Due to a strong vertical motion (Figures 1b1-1b4), the particle size in the convective core is generally larger or equal to 2.8 mm (Figures 1c1-1c4). However, the particles became smaller towards the end of convective region with the increasing particle number (Figures 1d1-1d4). The region just behind the

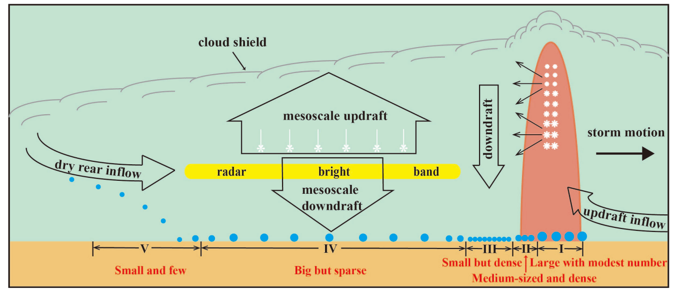

Figure 3. Conceptual model of squall-line MCS. See the text for further explanation.

squall line is called "transition zone" because it is a "reflectivity trough" (usually < 35 dBZ near the surface). Apparently, most smaller particles are concentrated in this region (Figures 1b1-1b4). Behind the transition zone, the bright band extends to a large area, and the maximum reflectivity can reach 50 dBZ in some cases. In the heavy stratiform area, the particle size D_m is normally larger than 1.2 mm at the storm top, and gradually grows up to more than 2 mm near the surface, making this region stand out in the surrounding areas as shown in Figures 1c1-1c4. On the other hand, the heavy stratiform area is also characterized by the scarce particle number concentration (Figures 1d1-1d4). Noting that the reflectivity factor $Z = \int_0^{+\infty} D^6 N(D) dD$, the radar reflectivity is much more sensitive to the particle size rather than the number, which explains the strong reflectivity in heavy stratiform area and the weak radar echo in the transition zone. Behind the heavy stratiform region, the reflectivity is decreased due to the reduced particle size even though the number of the particles is slightly increased.

The squall line is divided into five regions, i.e., mature cells, old cells, transition zone, heavy stratiform and stratiform tail as shown in Figure 1, mainly based on the vertical section of reflectivity (Figure 1b1-b4) that implies different microphiscal processes in the cloud. The convective and stratiform regions are firstly distinguished according to the vertical variation of reflectivity. For the stratiform, the region with intense bright band (e.g., > 40 dBZ) is identified as the heavy stratiform (region IV), and the areas in front of and behind it are segregated into the transition zone (region III) and stratiform tail (region V), respectively. The old cells (region II) are characterized with the obviously reduced altitude where the reflectivity of 45 dBZ can reach and the markedly increased N_t (Figure 1d1-d4) at different altitudes. Finally, the remain area in the convective is identified as the mature cells (region I). Figure 2 shows the vertical profiles of Ku-band reflectivity and PSD among the five regions with each row corresponding to one squall line event in Figure 1. Mature cells show the strong reflectivity (typically > 50 dBZ near the surface) because of the large particle size—the D_m is usually larger than 2.5 mm near the surface—but the magnitude of N_t and its horizontal distribution vary with events (Figure 1d1-1d4). As shown in Figure 2c1-c4, the averaged N_t could be the lowest, moderate or largest among five regions. The particles in old cells decrease greatly in size. However, the intensity of reflectivity is still very high (typically > 40 dBZ near the surface) mainly because of the increased number of medium-size particles. The smallest particles are concentrated in the transition zone where they produce a “reflectivity trough” despite the higher N_t. For the heavy stratiform region, the reflectivity increases to about 40 dBZ because the particles become larger. The D_m of the raindrops is about 2.0 mm, which could grow up to 2.5 mm in intense squall lines (Figure 2b4). On the other hand, N_t in this region is obviously the smallest. For the stratiform tail, the reflectivity is usually less than 30 dBZ due to the rapidly decreased particle size, but the N_t is slightly higher than that in the heavy stratiform area.

The studies of mesoscale air motions during squall lines have been reviewed by Houze 2004 [2]. In brief, in front of the convective cells, an air flow originated in low levels ascends through the convective and further into stratiform regions. There is a downdraft from middle to low levels in the transition zone, and a mesoscale updraft in upper levels and downdraft from middle to low levels can be found in the heavy stratiform region. Besides, a cold dry rear inflow is a distinct feature of squall-line MCS’s. Combining the wind fields and the DPR PSD, we have made some revisions to the model in BH91 (see their Figure 18) and present a revised conceptual model (Figure 3). In BH91, the trajectories of precipitating particles were estimated from the wind fields using the observations of many different instruments and the particle fall speeds were derived from a fall speed – reflectivity relationship in the convective region and the doppler data in the stratiform region. According to the estimated particle trajectories, BH91 speculated that the falling positions of the hydrometeors coming from the convective region mostly depend on the altitude where they would be cast rearward, and the number of casting at lower levels would be less than that at higher levels. Thus the transition zone could be illustrated using few raindrops. Accordingly, many more precipitating particles would be cast farther, and formed the heavy stratiform. However, the DPR observations are quite different (Figure 1 and 2).

In our conceptual model, the particles in mature cells are not very dense but have a larger size than those in old cells like BH91. There are smaller particles in the old cells like the corresponding area in BH91, but in larger quantities instead. We infer that the detrainment of hydrometeors from the convective region by the updraft inflow would not be as orderly as described in BH91, but be more complex and disordered. The ice particles being cast at different levels are possible to fall into the vicinity, hence most hydrometeors are concentrated in the old cells and transition zone because they have a wider source of the casting. Due to the shorter distance of the rearward dispersion that allows the less aggregation and vapor deposition, the raindrops in the transition zone have smaller diameters. However, the D_m in old cells is larger than that in the transition zone, likely because the particles in old cells is a mixture of larger particles that fall faster and much smaller particles from mature cells. Moreover, the downdraft in mid-to-low levels above the transition zone may evaporate the hydrometeors to some extent and reduce the chance of particle growth by accelerating their subsidence. As the casting distance increases, precipitating particles can get larger since more aggregation and water vapor deposition may take place. The heavy stratiform area stands out with a distinct PSD characteristic. It is noted that the particles in this region are apparently sparse from storm top to the surface, but the particle size is much larger even at the upper levels. Besides, in this region, the ice particle size above the freezing level grows much faster than it does in the transition zone and the stratiform tail in the vertical direction. We therefore speculate the mesoscale updraft occurring at the upper levels might greatly promote the growth process of ice particles. The vapor diffusion promoted by the mesoscale updraft is conducive for ice crystals to stick together when they collide (aggregations). Moreover, a strong and consistent updraft can slow down the falling of hydrometeors and facilitate mutual collisions (collisions-coalescences). As a result, those particles entering this updraft-dominating region are most likely to grow to a considerable size while still remaining at the relatively high levels. The number of those particles would reduce accordingly. Or, from another perspective, because of the existence of mesoscale ascending airflow, only the larger ice crystals with faster falling speeds finally might fall down to the surface in this region while those smaller particles might be advected to the rear. Furthermore, as the effect of mesoscale updraft wears off backward the heavy stratiform area, the number of hydrometeors would slightly rise in most cases. In the further rear, the dry rear inflow could evaporate the hydrometeors, especially for the rear edge of the stratiform region where the air flow be very strong. Therefore, the hydrometeors would get smaller and smaller towards the end of heavy stratiform region.

IV. Summary And Future Work

In this paper, we take an insight into squall-line MCS’s by employing dual-frequency retrievals of DPR observations. The PSD characteristics, represented by the mass-weighted mean diameter (D_m) and the total particle number concentration (N_t) in vertical cross section are investigated. Based on the observations, a revised conceptual model is proposed. Although the GPM DPR retrieval errors might be an issue, the error analysis and algorithm validataion are beyond the scope of current study. Given the validation results from many other GPM DPR studies, the accuracy of PSD retrievals is believed to support the analysis of proposed conceptual model.

In our conceptual model of squall-line MCS, the convective region is separated into mature cells and old ones based on different PSD characteristics. The particle size in the mature cells is large, but with modest number, while the particle size in the old cells is comparatively smaller with higher particle number. The major difference between the revised conceptual model and BH91 is the particle number concentrations in the transition zone and the heavy stratiform region. DPR retrievals show a high concentration of smaller particles in the transition zone. The minimum particle concentration is found in the heavy stratiform region. In view of DPR observations, we speculate that the rearward detrainment of hydrometeors from the convective region should be mixed, and the particles at all different levels would have the chance to fall into the transition zone. The hydrometeors falling into the tailing stratiform region should be mainly from the higher levels . The mesoscale updraft appearing at the upper levels of heavy stratiform region might promote the aggregations and collisions-coalescences of ice crystals, and consequently could prompt the growth of particle size but reduce the particle number.

In the future, we will further look into the microphysical mechanism in the stratiform region, and focus on the following aspects that remain unclear in the current work: (1) Why the transition zone has the highest concentration of particles? (2) Whether the mesoscale updraft occurring at the upper levels in the heavy stratiform can promote the growth of particle size? If so, to what extent it may contribute to the growth of particle? (3) Whether the rear dry inflow can decrease the particle size? To unveil these physical mechanisms, more observations are needed, such as direct observations by instrumented aircraft, dual-polarimetric radar and disdrometer observations.

ACKNOWLEDGMENT

We would like to thank the scientists and those who contribute to the GPM mission. The dual-frequency2A-DPR data of GPM used in this study are available online (https://storm.pps.eosdis.nasa.gov/storm/). Major funding for this research was provided under National Key Research and Development Project (2016YFC0400902 and 2018YFC1507505), Strategic Priority Research Program of Chinese Academy of Sciences (Grant No. XDA2006040101) and Hundred Talent Program.

REFERENCES

[1] C. A. Doswell, H. E. Brooks, and R. A. Maddox, “Flash flood forecasting: an ingredients-based methodology,” Weather and Forecasting, vol. 11, pp. 560-581, 1996.

[2] R. A. Houze, “Mesoscale convective systems,” Reviews of Geophysics, vol. 42, no. 4, 2004.

[3] B. J. Moore, P. J. Neiman, and M. F. Ralph, “Physical process associated with heavy flooding rainfall in Nashville, Tennessee, and vicinity during 1-2 May 2010: The role of an atmospheric river and mesoscale convective systems,” Monthly Weather Review, vol. 140, pp. 358-378, 2012.

[4] R. S. Schumacher, and R. H. Johnson, “Organization and environmental properties of extreme-rain-producing mesoscale convective system,” Monthly Weather Review, vol. 133, pp. 961-976, 2005.

[5] R. A. Houze, “100 Years of Research on Mesoscale Convective Systems,” Meteorological Monographs, vol. 59, pp. 17.1-17.54, 2018.

[6] D. M. Wheatley, N. Yussouf, and D. J. Stensrud, “Ensemble Kalman Filter Analyses and Forecasts of a Severe Mesoscale Convective System Using Different Choices of Microphysics Schemes,” Monthly Weather Review, vol. 142, no. 9, pp. 3243-3263, 2014.

[7] B. Chen, J. Wang, and D. Gong, “Raindrop Size Distribution in a Midlatitude Continental Squall Line Measured by Thies Optical Disdrometers over East China,” Journal of Applied Meteorology and Climatology, vol. 55, no. 3, pp. 621-634, 2016.

[8] M. Maki, T. D. Keenan, Y. Sasaki et al., “Characteristics of the raindrop size distribution in tropical continental squall lines observed in Darwin, Australia,” Journal of Applied Meteorology, vol. 40, pp. 1393-1412, 2001.

[9] S. Moumouni, M. Gosset, and E. Houngninou, “Main features of rain drop size distributions observed in Benin, West Africa, with optical disdrometers,” Geophysical Research Letters, vol. 35, no. 23, 2008.

[10] R. Cifelli, C. R. Williams, D. K. Rajopadhyaya et al., “Drop-size distribution characteristics in tropical mesoscale convective systems,” Journal of Applied Meteorology, vol. 39, pp. 760-777, 2000.

[11] A. Y. Hou, R. K. Kakar, S. Neeck et al., “The Global Precipitation Measurement Mission,” Bulletin of the American Meteorological Society, vol. 95, no. 5, pp. 701-722, 2014.

[12] M. I. Biggerstaff, and R. A. Houze, Jr., “Kinematic and precipitation structure of the 10-11 Jun 1985 squll Line,” Monthly Weather Review, vol. 119, pp. 3034-3065, 1991.

[13] R. A. Houze, Jr., “Observed structure of mesoscale convective systems and implications for large-scale heating,” Quarterly Journal of the Royal Meteorological society, vol. 115, pp. 425-461, 1989.

[14] R. A. Houze, Jr., S. A. Rutledge, M. I. Biggerstaff et al., “Interpretation of doppler weather radar displays of midlatitude mesoscale convective systems,” Bulletin American Meteorological Society, vol. 70, pp. 608-619, 1989.

[15] T. Iguchi, S. Seto, R. Meneghini et al., “GPM/DPR Level-2 Algorithm Theoretical Basis Document,” 2018.

[16] L. P. D’Adderio, G. Vulpiani, F. Porcù et al., “Comparison of GPM Core Observatory and Ground-Based Radar Retrieval of Mass-Weighted Mean Raindrop Diameter at Midlatitude,” Journal of Hydrometeorology, vol. 19, no. 10, pp. 1583-1598, 2018.

[17] L. Liao, R. Meneghini, and A. Tokay, “Uncertainties of GPM DPR Rain Estimates Caused by DSD Parameterizations,” Journal of Applied Meteorology and Climatology, vol. 53, no. 11, pp. 2524-2537, 2014.

[18] L. Liao, and R. Meneghini, “Physical Evaluation of GPM DPR Single- and Dual-Wavelength Algorithms,” Journal of Atmospheric and Oceanic Technology, 2019.

[19] W. Petersen, M. Thurai, P. Gatlin et al., “Consistent measurement and physical character of the DSD: Disdrometer to satellite,” 2017. (https://ntrs.nasa.gov/archive/nasa/casi.ntrs.nasa.gov/20170010664.pdf)

[20] Radhakrishna. B, S. K. Satheesh, T. Narayana Rao et al, “Assessment of DSDs of GPM-DPR with ground-based disdrometer at seasonal scale over Gadanki, India,” 2016, Journal of Geophysical Research: Atmospheres, 121(19), 11-792.

[21] S. Seto, T. Iguchi, and T. Oki, “The Basic Performance of a Precipitation Retrieval Algorithm for the Global Precipitation Measurement Mission's Single/Dual-Frequency Radar Measurements,” IEEE Transactions on Geosciences and Remote Sensing, vol. 51, pp. 5239-5251, 2013.